

# Chapter 85

## Study on Damage Identification of Reinforced Concrete Members Based on BP Neural Network



Yudong Zhang, Zuanfeng Pan, and Jianyu Qin

**Abstract** Structural damage identification plays an important role in the performance evaluation and maintenance of existing structures and post-disaster damaged buildings. On the basis of summarizing and analyzing the commonly used damage models of concrete structures and the description of structural safety state in domestic and foreign codes, a method of damage index fitting and safety state identification for reinforced concrete flexural members based on BP neural network is proposed in this study. Two independent BP neural network damage models for damage index fitting and safety state recognition, respectively, are established using Matlab. For the damage index fitting, this method takes the crack characteristic parameters as the input of the network, and the damage index calculated by the dual-variable damage model based on stiffness and energy is regarded as the output. For the safety state recognition, the proposed method takes the crack characteristic parameters as the input and the safety state classification result following the FEMA-356 code serves as the output. Thereby, the mapping relationship between the crack characteristic parameters and reinforced concrete member damage can be established. Compared with the traditional damage assessment methods, this proposed method has the advantages of accuracy, promptness and convenience, and it enriches the technical means of structural health monitoring.

**Keywords** Concrete · Crack · Neural network · Damage identification

---

Y. Zhang · Z. Pan  
College of Civil Engineering, Tongji University, Shanghai 200092, China

J. Qin (✉)  
Creentown China Holdings Limited, Hangzhou 310000, China  
e-mail: [qinjianyu\\_tj@163.com](mailto:qinjianyu_tj@163.com)

## 85.1 Introduction

During the service life of reinforced concrete structures, irreversible material aging and structural damage will occur due to factors such as structural conditions and environmental erosion. The damage accumulates and leads to degradation in structural performance, causing a decrease in bearing capacity and durability and endangering the structure. Structural damage can be categorized as sudden or cumulative. The former is caused by sudden natural disasters or man-made events, which is unpredictable. The latter is caused by internal damage and crack propagation resulting from environmental erosion and structural aging, which is more concealed and dangerous. The purpose of structural damage identification is to determine whether damage has occurred, its location and degree, and analyze the impact of damage on the structure. It provide a basis for the health and lifespan prediction of the structure.

Traditional damage detection methods include appearance inspection for defects such as cracks, deformation, and local damage, as well as non-destructive testing using instruments such as ultrasonic waves, infrared cameras [1], and acoustic emission. However, the effectiveness of detection is influenced by the professional knowledge and engineering experience of the personnel. Structural damage identification based on static response involves measuring displacement, strain and other static response information through on-site load testing, and obtaining static parameters (such as stiffness, elastic modulus) of the structure. However, currently the detection equipment is bulky and can affect the normal operation of the structure, making online measurement difficult to achieve [2]. Currently, damage identification based on dynamic characteristics is a hot research topic, including methods such as dynamic fingerprinting [3], model updating [4], and neural network [5]. Among them, dynamic fingerprinting is a structural damage identification method based on modal parameters. By detecting changes in dynamic indicators (frequency, mode shape, modal curvature, strain mode, etc.), it can indicate whether damage has occurred, the degree of damage, and the location of damage in the structure. Currently, damage identification methods based on multiple modal parameters have been developed [6]. The model updating method is an important approach for damage identification. In this method, a finite element model of the structure is established first, and then damage identification is converted into a model optimization problem under constraint conditions. By continuously adjusting and modifying the parameters of the original model [7], such as the stiffness matrix, the results can eventually become consistent with the actual structural response, achieving the effect of damage identification. The neural network method [8–10] is a type of damage identification method based on artificial intelligence. In this method, a damage identification network model is trained through sample data, and then it is used to diagnose damage in structures. It is non-parameter and suitable for large-scale nonlinear systems. It also has good fault-tolerance and robustness, and is widely used in damage identification of structures.

This article proposes a damage index fitting and safety state assessment method for reinforced concrete components based on the basic principles of BP neural network.

It takes surface crack information of concrete components as the damage identification parameter, and construct two BP neural network damage models for damage index fitting and safety state recognition, thereby establishing a mapping relationship between crack feature parameters and component damage. This method has the advantages of accuracy, promptness and convenience. It enriches the technical means of structural health monitoring and provides important decision-making basis for timely evaluation of existing structures' usage conditions and formulation of maintenance measures. It also provides a fast, non-destructive, and practical method for health diagnosis and safety state assessment of post-disaster buildings.

## 85.2 The Damage Index and Safety State Assessment of Concrete Structures

### 85.2.1 *Damage Index and Damage Parameters*

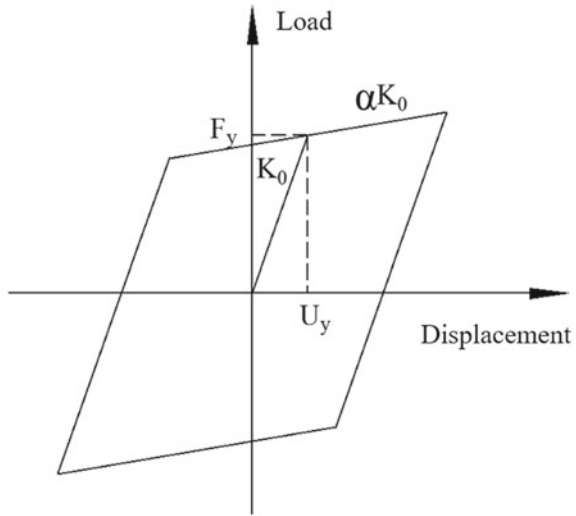
Concrete structures subjected to seismic loading experience various levels of damage. This damage can be observed at a macroscopic level as an expansion of microcracks within the concrete structure, adhesive effects between materials, and a decrease in stiffness and strength of material. Additionally, the structure enters the nonlinear stage due to the plastic deformation, leading to a decrease in overall stiffness and bearing capacity and an increase in overall ductility. For instance, the elastic–plastic restoring force model shown in Fig. 85.1 shows that when the structural elastic force caused by seismic activity exceeds the yield load, the structure enters a plastic state, with decreased stiffness and increased ductility. The input energy of the structure gradually dissipates during the hysteresis process, where the ductility increases and the accumulated damage to the structure increases. Therefore, the stiffness, ductility, and hysteresis energy of the structure can indicate the degree of damage, and are often referred to as damage parameters.

From a microscopic perspective, structural damage is accompanied by the accumulation of plastic strain, plastic strain energy, plastic displacement, and plastic energy dissipation. Therefore, plastic strain and plastic strain energy can also be used as damage parameters to describe the degree of damage. However, in actual situation, macroscopic damage parameters are more practical, and easier to obtain than microscopic parameters. Therefore, using stiffness, displacement, and energy as damage parameters to quantitatively describe the degree of damage is a more practical method.

For the quantitative evaluation of the degree of damage of concrete structures or components, damage indices  $D$  can be used. The damage index is a dimensionless parameter defined as:

$$D = f(x_1, x_2, x_3 \cdots, x_n) \quad (85.1)$$

**Fig. 85.1** The elastic–plastic restoring force model



where  $x_1, x_2, x_3 \dots, x_n$  are the damage parameters, such as stiffness, displacement, energy, strain, stress, etc., which reflect the mechanical properties and damage of the structure, and can be directly measured or calculated by instruments.

$f(\cdot)$  is the damage model, which is the mapping relationship between the damage parameter and the damage index.

The damage index  $D$  has the following characteristics [11, 12]:

- (1)  $D \in [0, 1]$ ,  $D = 0$  indicates no damage to the structure, while  $D = 1$  indicates complete failure, and  $0 < D < 1$  indicates partial damage to the structure.
- (2) The damage index  $D$  increases gradually with the increase of the service life of the structure, and the overall trend of the increase is irreversible.

## 85.2.2 Damage Models of Concrete Structures

A damage model is a mathematical expression used to characterize the extent of damage to a structure [13]. Currently, various damage models for concrete structures have been proposed to evaluate the effects of cumulative low-cycle fatigue loads on structural damage. Based on the number of damage parameters, damage models can be classified into single-parameter and multi-parameter models, while based on the type of damage parameter, they can be divided into displacement-based, energy-based, and displacement-energy-based models. This paper summarizes several commonly used damage models and their characteristics, as shown in Table 85.1.

In summary, different types of damage models can produce different results for the damage evolution process of the same structure, and the assessment of the damage

**Table 85.1** Commonly used damage models

Type	Characteristics	Researcher	Damage model
Single-parameter	Displacement-based	Powell [14]	$D_P = \frac{U_i - U_y}{U_u - U_y}$
		Newmark [15]	$D_N = \sum_{i=1}^N (\mu_{i,max} - 1)$
		Krawinkler [16]	$D_K = \sum_{i=1}^N (\mu_i - 1)^b$
		Mehanny [17]	$D_M = (U_{i,max})^\alpha + \left( \sum_{i=1}^N U_i \right)^\beta$
	Energy-based	Darwin [18]	$D_D = \sum_{i=1}^N \frac{E_i}{F_y(U_u - U_y)}$
		Gosain [19]	$D_G = \sum_{i=1}^N (\mu_i - 1)\lambda_i$
		Ibarra [20, 21]	$D_I = \sum_{i=1}^N \left( \frac{E_i}{E_t - \sum_{j=1}^i E_j} \right)^\alpha$
Stiffness-based	Gulkan [22]	$D_G = 1 - \frac{K_s}{K_0}$	
Multi-parameter	Displacement-energy-based	Park-Ang [23]	$D_{PA} = \frac{U_m}{U_u} + \beta \frac{\sum_{i=1}^N E_i}{F_y U_u}$
		Ou et al. [24]	$D_{OU} = \left( \frac{U_i}{U_u} \right)^\beta + \left( \frac{\sum_{i=1}^N E_i}{E_u} \right)^\beta$
		Banon [25]	$D_B = \sqrt{(\mu_{i,max} - 1)^2 + \left( \sum_{i=1}^N h \left( 2 \cdot \frac{E_i}{F_y U_u} \right)^d \right)^2}$

Note  $E_i$  is the energy dissipated by structure in the  $i$ th cycle;  $E_t$  is the total energy of the structure;  $E_u$  is the ultimate energy dissipated by the structure under monotonic loading;  $U_i$  is the maximum deformation in the  $i$ th cycle of the structure;  $U_u$  is the ultimate deformation value of the structure under monotonic loading;  $U_y$  is the yield deformation of the structure;  $F_y$  is the yield load of the structure;  $K_s$  is the secant stiffness of the structure;  $K_0$  is the initial stiffness of the structure;  $\mu_i$  is the ductility coefficient, defined as  $\mu_i = U_i / U_y$ ;  $\lambda_i$  is the ductility ratio, defined as  $\lambda_i = F_i / F_y$

state of the same structure may also differ. Therefore, for components with different types and failure modes, the damage model should be selected accordingly.

### **85.2.3 The Assessment of Safety State for Concrete Structure**

In general, damage index represents the degree of damage to a structure or component. The larger the damage index of a structure, the lower its remaining performance level and the worse its safety state. Conversely, the smaller the damage index of a structure, the higher its remaining performance level and the better its safety state. However, different researchers have different ideas of how to correspond quantitative damage index to safety state. This paper uses the Park-Ang damage model, Ou's damage model, and Tan's two-parameter damage model as examples. Table 85.2 shows the corresponding relationship between damage index and safety states.

Damage index can quantitatively describe the safety state of a structure or component, but in practical applications and regulations, more intuitive and measurable damage parameters are usually selected as parameters for damage evaluation and safety assessment. Generally, the structural apparent cracking condition and inter-story drift are selected as qualitative and quantitative evaluation standards. Among such regulations, the more representative ones are the Turkish regulation TBEC 2018 and the US regulation FEMA 356. The Turkish regulation TBEC-2018 pays more attention to the inter-story drift angle for structural safety state classification. The US regulation FEMA 356 comprehensively considers the apparent damage of the component and inter-story drift, and individually evaluates the damage of primary and secondary components. Tables 85.3, 85.4 provide some safety assessment standards in the above two regulations.

## **85.3 Damage Identification of RC Structures Based on BP Neural Network**

### **85.3.1 The Construction of BP Neural Network**

The basic theory of the BP neural network has been extensively introduced in previous literature. In this section, we will create two neural networks based on the design theory for the damage identification method using surface crack parameters of concrete. The two neural networks are respectively used for numerical simulation of damage index and recognition of safety states. Table 85.5 provides the structural parameters for both BP neural networks, and Fig. 85.2 shows the neural network structure diagram created in MATLAB.

It is worth noting that the input layer of both neural networks has 4 nodes, and the input vectors are  $[x_1, x_2, x_3, x_4]$ , representing 4 real damage parameters: crack length, maximum width, average width, and crack area.

In the numerical simulation of damage indicators, the initial number of hidden layers is 2, with 10 nodes in the first layer and 5 nodes in the second layer. During the actual training process, the number of layers and nodes can be dynamically adjusted based on the quantity and quality of training samples, in order to achieve the best

**Table 85.2** Corresponding relationship between damage index and safety states of RC structure

Damage model	Safety state				
	Intact	Mild damage	Moderate	Severe damage	Collapse
Park-Ang	$0 < D_{PA} < 0.4$		$0.4 \leq D_{PA} < 1.0$		$1 \leq D_{PA}$
Ou's	$0 < D_{OU} < 0.1$	$0.1 \leq D_{OU} < 0.25$	$0.25 \leq D_{OU} < 0.45$	$0.45 \leq D_{OU} < 0.9$	$0.9 \leq D_{OU}$
Tan's [13]	$0 < D_{KE} < 0.1$	$0.1 \leq D_{KE} < 0.3$	$0.3 \leq D_{KE} < 0.65$	$0.65 \leq D_{KE} < 0.85$	$0.85 \leq D_{KE} \leq 1$

**Table 85.3** Assessment of safety state in TBEC 2018 [26]

Code	Structures/ Components	Safety state describe			
		Minimum damage	Significant damage	Extreme damage	Collapse state
TBEC-2018	RC column	$\delta/H < 1\%$	$1\% < \delta/H < 3\%$	$3\% < \delta/H < 4\%$	$4\% < \delta/H$

**Table 85.4** Assessment of safety state in FEMA 356 [27]

Structures/ Components	Safety State performance level		
	Immediate occupancy (S-1)	Life safety (S-3)	Collapse prevention (S-5)
Concrete frame shear wall structure	① Wall has fine cracks with a width less than 1/16 inch; ② Beam-to-column connections have cracks with a width less than 1/8 inch	① Some edge reinforcement yielded; ② Sliding and cracking have occurred at joints; ③ Wall has experienced spalling and flexural cracks, with concrete crushing, but generally in place	① Obvious flexural and shear cracks appeared; ② Sliding occurred; ③ Obvious concrete crushing and steel yielding; ④ Damage around openings
	① 0.5% inter-story drift; ② No permanent drift	① 1% inter-story drift; ② 0.5% permanent drift	① 2% inter-story drift; ② Or permanent drift

**Table 85.5** Parameters of the neural network

Function	Input layer vector	Output layer vector	Hidden layer numbers	Nodes number in hidden layer
Damage index	$[x_1, x_2, x_3, x_4]$	$y$	2	[10, 5]
Safety states	$[x_1, x_2, x_3, x_4]$	[1, 0, 0, 0], [0, 1, 0, 0], [0, 0, 1, 0], [0, 0, 0, 1]	1	10

mapping process. The transfer function of the output layer adopts the 'logsig' function to ensure that the output vector (damage index) is between 0 and 1. The number of nodes in the output layer is 1, and the output vector  $y$  represents the magnitude of the damage index.

In the safety state recognition network, the initial setting for the number of hidden layer is 1, and the output layer has 4 nodes, with an output vector of a  $1 \times 4$  array composed of 0 and 1. Each vector represents the different safety state. For example,



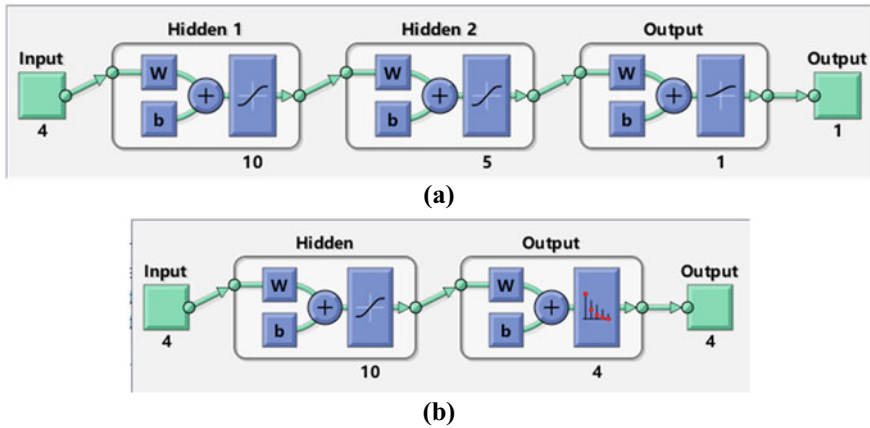


**Fig. 85.2** The structure of the neural network in MATLAB: **a** the neural network for numerical simulation of damage index, **b** the neural network for recognition of safety states

[1, 0, 0, 0] represents the first stage of the safety state, which in TBEC 2018 specification represents a mild damage state, and in FEMA 356 specification represents a directly inhabitable state.

### 85.3.2 The Calculation of Input and Output Vectors in BP Neural Network

The calculation of input vector  $[x_1, x_2, x_3, x_4]$  can be obtained by processing a series of shear wall images under different loading displacements, and calculating the crack parameters based on computer vision (refer to Sect. 4.4.1 for details). As for output vector  $y$ , it is calculated based on the hysteresis curve during the component loading process and the multi-parameter model based on stiffness and energy [13]. The determination of output vector  $[1, 0, 0, 0], [0, 1, 0, 0], [0, 0, 1, 0], [0, 0, 0, 1]$  is based on maximum drift capacity and apparent damage parameters for safety states classification in the FEMA-356. Finally, the corresponding relationship between input vector and output vector is established to construct a data sample database for neural network training and learning.

### 85.3.3 Training and Validation

The process of damage identification using neural networks mainly consists of two stages: training and validation. The sample database is divided into two parts, with 70% to 80% of the data randomly selected for network training and the remaining

samples used for validation of the trained network. The recognition accuracy of the neural network is calculated during validation. To maximize the recognition performance of the network, the proportion and size of training samples can be adjusted, and the capacity and quality of the sample database can be improved. Additionally, based on the recognition performance of the network, the number of hidden layers and nodes in the network can be adjusted systematically to gradually improve the recognition performance, achieving the best recognition accuracy.

## 85.4 Experimental Verification

In order to verify the feasibility and accuracy of the neural network model proposed in the previous chapter, this section selected the more complex neural network structure model used for damage index fitting (Fig. 2a) for test verification. The test object of this test is the reinforced concrete shear wall. Through the pseudo-static test of the shear wall, the damage degree and crack development of the member during its failure process were studied. Firstly, a camera was set up to photograph the cracks on the shear wall surface, and the corresponding crack parameters were further extracted. Secondly, the damage index of shear wall in the loading process was calculated by using the hysteretic curve of the component. Finally, the test data was selected for neural network training to realize damage identification of the shear wall.

### 85.4.1 Test-Piece Parameter

The test object of this test is reinforced concrete cast-in-place shear wall, and the test-piece is composed of concrete base, concrete wall body and wall top loading beam, which is referred to as S1. Its design parameters are shown in Table 85.6. HRB400E is used for the steel bar of the test-piece, C30 is used for the concrete, and the main mechanical properties of the material are shown in Table 85.7.

**Table 85.6** Design parameters of concrete shear wall

Member	Wall body (mm)	Loading beam (mm)	Shear span ratio	Axial compression ratio
S1	160 × 1400 × 2800	400 × 250 × 1800	2.0	0.25

**Table 85.7** Main performance indexes of materials (unit: MPa)

Concrete				Steel bar		
$f_t$	$f_c$	$f_{cu}$	$E$	$f_y$	$f_u$	$E$
2.74	28.46	42.55	$3.2 \times 10^4$	335.41	490.20	$2.03 \times 10^5$

### **85.4.2 Loading Device and Loading System**

The horizontal load was applied by a 1000kN electro-hydraulic servo actuator mounted on the reaction wall. The force was concentrated in the center of the beam. The vertical load was provided by the 2500kN hydraulic jack distributed at the top of the loading beam. The force of the hydraulic jack was reacted on the top of the loading beam after passing through the reaction frame. In addition, the loading of the test-piece includes two parts: pre-loading and formal loading.

#### *Pre-Loading*

It is used to test whether the contact between the loading device and the shear wall member is good, whether the measuring instrument is accurate, and the preload value should be less than 30% of the cracking load. After several pre-loadings, the formal loading can be implemented only after the loading device, specimen and measuring instrument work normally.

#### *Formal Loading*

It mainly includes the vertical axial pressure exerted by the hydraulic jack and the horizontal load exerted by the actuator. The axial pressure exerted by the vertical hydraulic jack can be calculated by converting the axial pressure ratio. The horizontal load applied to the top of the loading beam is provided by the actuator. The loading system adopted load–displacement hierarchical loading with load first and displacement hierarchical loading later. Since the shear wall is in the elastic stage in the early stage and the specimen stiffness is relatively large, the load grading loading stage was adopted before the cracking of the specimen. In this way, it's easier to capture the cracking, yield and other characteristic points of the component when loading with load control. After yielding, the specimens were changed to displacement grading loading mode, and the maximum displacement  $\Delta$  at yield was taken as the unit displacement for graded loading. The loading displacements were  $1\Delta$ ,  $2\Delta$ ,  $3\Delta$ ... And the loading cycle is repeated three times for each stage of displacement until the specimen is damaged or the load drops to 85% of the maximum load.

### **85.4.3 Measuring Device and Measuring Method**

In the measurement system, Canon EOS800D was used for the camera, and the parameter information is shown in Table 85.8. The focal length of the camera and the position height of the tripod were adjusted to ensure that the shear wall was always within the image range during the loading process. It should be noted that once the camera position and parameters have been adjusted, the camera cannot be adjusted during the loading process to ensure that the resolution of the image is unique. In addition, in order to ensure the sufficiency and stability of the environmental light

**Table 85.8** Camera parameters

Parameter	Form	Degree of freedom
Intrinsic parameter	$\mathbf{M}_1 = \begin{bmatrix} f_x & 0 & u_0 & 0 \\ 0 & f_y & v_0 & 0 \\ 0 & 0 & 1 & 0 \end{bmatrix}$	4
Radial distortion Tangential distortion	$k_1, k_2$ $p_1, p_2$	4
Extrinsic parameter (Rotation matrix and translation vector)	$\mathbf{R} = \begin{bmatrix} r_1 & r_2 & r_3 \\ r_4 & r_5 & r_6 \\ r_7 & r_8 & r_9 \end{bmatrix}, \mathbf{T} = \begin{bmatrix} t_x \\ t_y \\ t_z \end{bmatrix}$	6

source, two ground lamps were used as supplementary light sources to project on the surface of the shear wall during the test. The test site is shown in Fig. 85.3.

In terms of measurement methods, calibration plates needed to be posted for calibration image shooting before formal loading, so as to facilitate the later resolution calculation and correction. During the formal loading process, the camera needed to take photos of the shear wall at the position where the maximum displacement

**Fig. 85.3** Test site

of each loading cycle is loaded, and classify the photos to facilitate the construction of the corresponding relationship between the pictures and the damage in the later stage.

### 85.4.4 Test Results and Analysis

#### Extraction of Test Results

##### *Crack Parameter Identification*

Based on the shear wall images under different loading displacements collected by the measurement system, crack parameters were identified and extracted from images under different loading displacements. Specific image processing processes include: image clipping, image graying, image enhancement, image smoothing, image binarization, morphological operation and main crack extraction. Based on the extracted main crack edges, the image crack parameters could be further identified and calculated.

##### (1) Crack length calculation

In this paper, the piecewise summation method was used to calculate the length of cracks. This method uses the idea of differentiation and selects the coordinates  $(x_k, y_k)$  of different positions on the crack skeleton in the image with the mouse, so as to divide the whole crack into  $n$  short cracks, and then carries out approximate calculation for each segment according to the length formula of line segments.

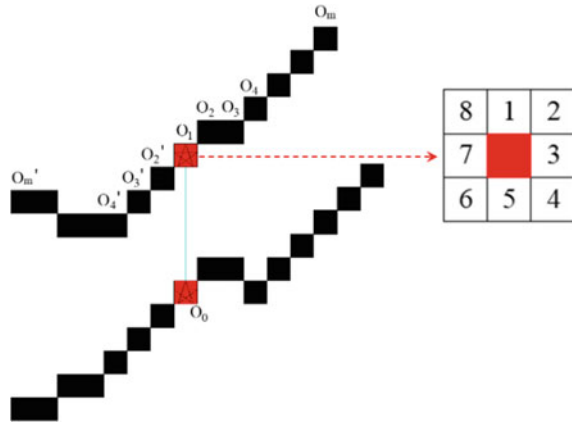
$$L = \alpha \times \sum_{k=1}^n \sqrt{(x_{k+1} - x_k)^2 + (y_{k+1} - y_k)^2} \quad (85.2)$$

where:  $\alpha$  is the image resolution, which can be obtained through image calibration, and  $(x_k, y_k), (x_{k+1}, y_{k+1})$  is the image coordinates of the  $k$  and  $k + 1$  points taken by the mouse point. The segmental calculation method does not need to burr the fracture skeleton curve, so it has the characteristics of convenient calculation and strong adaptability. Meanwhile, the method also has the advantages of strong visualization degree and high calculation accuracy, which can better meet the needs of practical engineering.

##### (2) Crack width calculation

This paper adopted the crack width calculation method based on local crack edge search, as shown in Fig. 85.4. The specific calculation process is as follows:

**Fig. 85.4** Schematic diagram of crack width calculation



- ① Extract the crack edge and locate the position coordinates  $(i_1, j)$ ,  $(i_0, j)$  of the upper and lower edge points  $O_1$  and  $O_0$  of the first row of the crack in column  $j$ .
- ② Take  $O_1$  as the center, search the gray values at positions 2–5 in the 8 neighborhood in the clockwise direction, label the first crack point found as  $O_2$ , and calculate the distance  $|O_0O_2|$  between  $O_0$  and  $O_2$ ;
- ③ Similarly, taking  $O_2$  as the center and repeating step ②, the point  $O_3$  and the distance  $|O_0O_3|$  can be obtained;
- ④ Repeat step ② and ③ to get the set  $L = \{|O_0O_1|, |O_0O_2|, \dots, |O_0O_m|\}$ ;
- ⑤ Take  $O_1$  as the center, search the gray values at positions 5–8 in the 8 neighborhood in the counterclockwise direction, label the first crack point found as  $O'_2$ , and calculate the distance  $|O_0O'_2|$  between  $O_0$  and  $O'_2$ ;
- ⑥ Similarly, taking  $O'_2$  as the center and repeating step ⑤, the point  $O'_3$  and the distance  $|O_0O'_3|$  can be obtained;
- ⑦ Repeat the steps ⑤ and ⑥ to get the set  $L' = \{|O_0O'_1|, |O_0O'_2|, \dots, |O_0O'_m|\}$ ;
- ⑧ The width of the crack in column  $j$  is  $\omega(j) = \min\{L, L'\}$ .

Based on the above method, by traversing the  $j$ -th column in step ① to all pixels of the extracted crack edges in the image, the maximum and average crack widths within the image range can be further obtained. It is worth noting that the above steps are aimed at transverse cracks. For vertical cracks, only the column operations in the above steps need to be converted into row operations.

(3) Crack area calculation

By counting the number of pixels in the crack area in the binary image and multiplying it with the image resolution, the crack area in the actual situation can be calculated, that is

$$S = n \times \alpha^2 \tag{85.3}$$

where:  $n$  is the number of pixels in the crack area in the image, and  $S$  is the actual area of the crack.

*Damage Index Calculation*

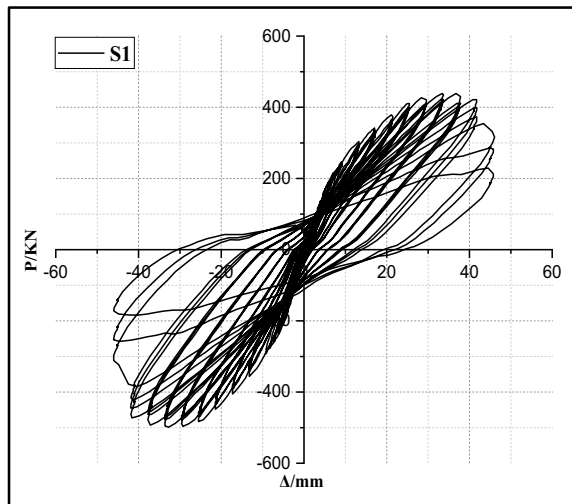
In terms of damage indexes selection, the two-parameter model based on stiffness and energy [13] was used in this paper to calculate the damage indexes. The model takes into account the effects of first surpassing failure and cumulative failure on the damage, and can better describe the evolution of structural damage under earthquake action. At the same time, the damage index of this model is stable between [0,1], and the quantitative evaluation of damage degree is more accurate. The damage model is:

$$D_{KE} = 1 - \left(1 - \frac{\int dE}{E_t}\right) \frac{K_i}{K_0} \tag{85.4}$$

where,  $\int dE$  is the cumulative energy consumption of the structure under a certain state,  $E_t$  is the total energy consumption of the structure,  $K_i$  is the secant stiffness of the structure under a certain state, and  $K_0$  is the initial elastic stiffness of the structure.

Figure 85.5 shows the hysteretic curve of component S1. Select the maximum displacement of each loading cycle, and calculate the damage index of its corresponding position using formula (85.4), so as to realize the assessment of shear wall damage degree.

**Fig. 85.5** Hysteretic curve of S1

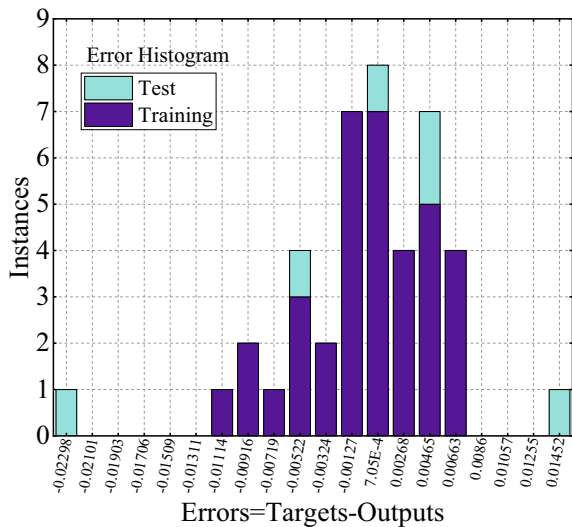


### Damage Identification

For the 53 groups of sample data extracted from S1 component, 42 groups were randomly selected for training and 11 groups were tested. The constructed neural network model was used to fit the damage index data of the above test results. From 42 groups of training samples, 70%, 15% and 15% were selected respectively for network training, verification and testing. The training algorithm adopted Levenberg–Marquardt algorithm, which is suitable for function approximation and fitting problems and has a fast training speed. In addition, in order to ensure that the network output meets the requirement that the damage index is between [0,1], the Log-Sigmoid function was used as the transfer function of the output layer. The training results are shown in Figs. 85.6, 85.7. The results show that with the increase of the number of iterations, the performance error (mean square error) of the neural network gradually decreases, and the training results of the neural network gradually tend to be stable. The mean square error of training and testing data is mainly distributed near zero, and the correlation coefficient  $R > 0.95$ , indicating that the training output of neural network can simulate the target output well, and the training effect of neural network is gratifying.

The 11 groups of test samples were input into the neural network completed with the above training, and the target output and actual output were compared and analyzed. The results showed that the identification accuracy of damage indicators of S1 component could reach 90.26%, and the neural network achieved the fitting effect of high accuracy damage indicators, as shown in Fig. 85.8.

**Fig. 85.6** Neural network error distribution statistical chart





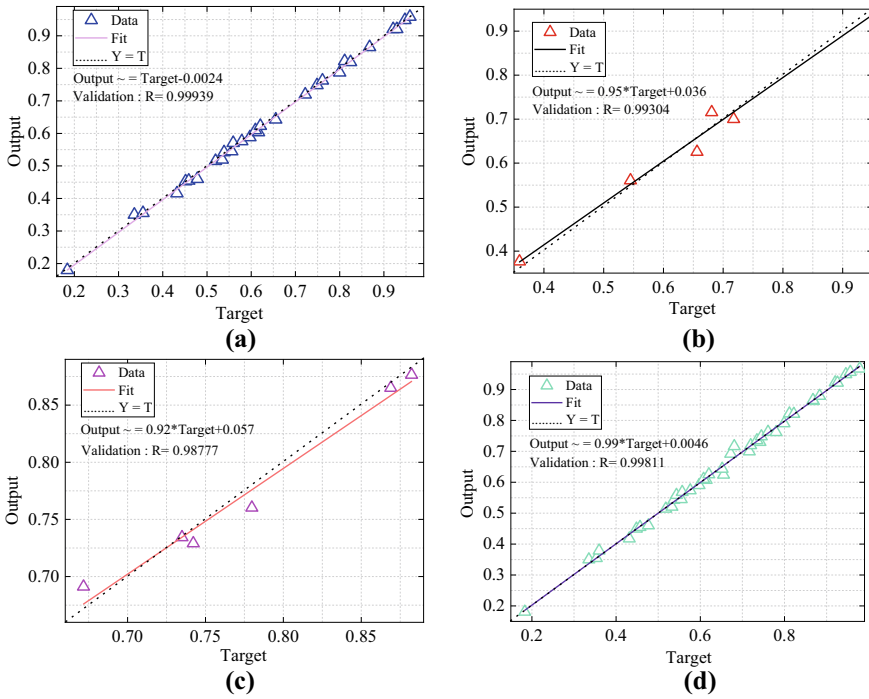
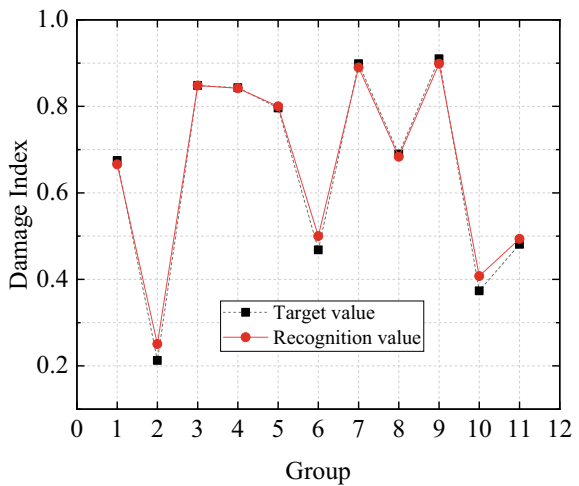


**Fig. 85.7** Fitting curve of damage index of neural network training group

**Fig. 85.8** Damage index identification results of the test group of component



## 85.5 Conclusion

On the basis of summarizing and analyzing the commonly used damage models of concrete structures and the description of structural safety state in relevant foreign codes, a method of damage index fitting and safety state identification for reinforced concrete members based on BP neural network is proposed in this study. This method takes surface crack information of concrete components as the damage identification parameter, and construct two BP neural network damage models for damage index fitting and safety state recognition, thereby establishing the mapping relationship between crack feature parameters and component damage. The method enriches the technical means of structural health monitoring and provides a fast, non-destructive method for health diagnosis and safety state assessment of damaged structures and post-disaster buildings. The main conclusions of this paper are as follows.

- (1) In the research of neural network damage identification, this paper proposes the method of damage index fitting and safety state identification for reinforced concrete members based on BP neural network, and designs multi-layer BP neural networks. For the damage index fitting, this method takes the crack characteristic parameters as the input of the network, and the damage index calculated by the dual-variable damage model based on stiffness and energy is regarded as the output. For the safety state recognition, the method takes the crack characteristic parameters as the input and the safety state classification result following the FEMA-356 code serves as the output. Therefore, the mapping relationship between the crack characteristic parameters and reinforced concrete member damage can be established.
- (2) In the aspect of surface crack parameter extraction of concrete members based on image processing technology, the applicability of commonly used image preprocessing algorithms and feature parameter extraction algorithms in concrete crack image recognition is studied in this paper. On this basis, for the calculation of the length of the crack, the segmented calculation method used in this paper does not need to deal with the burr noise of the crack skeleton curve. It has the characteristics of convenient calculation and strong adaptability. At the same time, the method also has the advantages of strong visualization and high calculation accuracy, which can better meet the needs of practical engineering. Crack width is one of the most important characteristic parameters in crack information, and it is also an important index affecting the quality of damage assessment. For the calculation of crack width, this paper starts from the definition of crack width and adopts the calculation method based on local crack edge search. This method avoids the problem that the calculated value becomes larger when the traditional tangent method is used to calculate the crack width at the place with a large crack curvature, thereby improving the recognition accuracy of the crack width.
- (3) In order to verify the feasibility and accuracy of the BP neural network method applied to the damage identification of reinforced concrete members, in this paper, the quasi-static loading test of shear wall is carried out for the neural

network model used for damage index fitting, which is more representative and more complex. The training results of the neural network applied to the damage index fitting of the shear wall in the test show that with the increase of the number of iterations, the performance error (mean square error) of the neural network gradually decreases, and the training results of the neural network gradually tend to be stable. The mean square error of training and testing data is mainly distributed near zero, and the correlation coefficient  $R > 0.95$ , indicating that the training output of neural network can simulate the target output well, and the training effect of neural network is gratifying. The damage index identification results of the test group of component S1 show that the identification accuracy of damage indicators of S1 component could reach 90.26%, and the neural network achieved the fitting effect of high accuracy damage indicators. The test results show good damage identification ability, which verifies the feasibility and accuracy of BP neural network method applied to damage identification of reinforced concrete members. The damage identification method of reinforced concrete members based on BP neural network proposed in this paper establishes the mapping mechanism between the apparent damage parameters and the damage index of the member, and realizes the identification process from the surface crack parameters of the concrete member to its internal damage.

**Acknowledgements** This research was supported by the National Key Research and Development Plan, China (2022YFC3801800).

## References

1. Liang, C.L.: Research status and prospect of structural damage identification. *Urban Constr. Theory Res.* **10**, 1–3 (2013)
2. Wu, X.N., et al.: Research status and prospect of bridge structure damage identification. *J. Chang'an Univ. (Nat. Sci. Ed.)* **33**(6), 49–58 (2013)
3. Sun, S., et al.: Identification of bridges' damage by dynamic fingerprints and Bayes data fusion. *J. Northeast. Univ. (Nat. Sci.)* **38**(2), 290–294 (2017)
4. Zhang, C., et al.: Structure damage identification by finite element model updating with Tikhonov regularization. *J. Nanchang Univ. (Eng. Technol.)* **32**(4), 394–398 (2010)
5. Narkis, Y.: Identification of crack location in vibrating simply supported beams. *J. Sound Vib.* **172**(4), 549–558 (1994)
6. Salawu, O.S., Williams, C.: Bridge assessment using forced-vibration testing. *J. Struct. Eng.* **121**(2), 161–173 (1995)
7. Tan, C.Y.: Application of deep learning in bridge health diagnosis. *Chongqing Jiaotong Univ., China* (2017)
8. Nakamura, M., et al.: A method for non-parametric damage detection through the use of neural networks. *Earthquake Eng. Struct. Dynam.* **27**(9), 997–1010 (1998)
9. Choi, M.Y., et al.: Damage detection system of a real steel truss bridge by neural networks. *Proceedings of SPIE-The International Society for Optical Engineering* **3988**, 295–306 (2000)
10. Wei, F.: Bridge damage identification based on dynamic parameters and bp neural network. *Anhui Jianzhu University, Hefei* (2019)

11. Li, H.Q.: Analysis and experiment of cumulated damage of steel frame structures under earthquake action. *J. Build. Struct.* **03**, 69–74 (2004)
12. Shen, Z., et al.: An experiment-based cumulative damage mechanics model of steel under cyclic loading. *Adv. Struct. Eng.* **1**(1), 39–46 (1997)
13. Tan, H.: Capacity spectrum method and an alternative damage model for seismic design of rigid frame tied-arch bridges. Southeast Univ., Nanjing (2007)
14. Powell, G.H., et al.: Seismic damage prediction by deterministic methods: concepts and procedures. *Earthquake Eng. Struct. Dynam.* **16**(5), 719–734 (1988)
15. Newmark, N.M., et al.: Fundamentals of earthquake engineering. Wiley Online Library, Hoboken, New Jersey (1972)
16. Krawinkler, H., et al.: Cumulative damage in steel structures subjected to earthquake ground motions. *Comput. Struct.* **16**(1–4), 531–541 (1983)
17. Mehanny, S.S.F., et al.: Seismic damage and collapse assessment of composite moment frames. *J. Struct. Eng.* **127**(9), 1045–1053 (2001)
18. Darwin, D., et al.: Energy dissipation in RC beams under cyclic load. *J. Struct. Eng.* **112**(8), 1829–1846 (1986)
19. Gosain, N.K., et al.: Shear requirements for load reversals on RC members. *J. Struct. Div.* **103**(7), 1461–1476 (1977)
20. Ibarra, L.F., et al.: Global collapse of frame structures under seismic excitations. Berkeley, CA: Pacific Earthquake Engineering Research Center, (2005)
21. Ibarra, L.F., et al.: Hysteretic models that incorporate strength and stiffness deterioration. *Earthquake Eng. Struct. Dynam.* **34**(12), 1489–1511 (2005)
22. Gulkan, P., et al.: Inelastic responses of reinforced concrete structure to earthquake motions. *J. Proc.* **71**(12), 604–610 (1974)
23. Park, Y., et al.: Mechanistic seismic damage model for reinforced concrete. *J. Struct. Eng.* **111**(4), 722–739 (1985)
24. Ou, J.P., et al.: Fuzzy dynamic reliability analysis and design of multi-story nonlinear aseismic steel structures. *Earthq. Eng. Eng. Vib.* **10**(04), 27–37 (1990)
25. Banon, H., et al.: Seismic damage in reinforced concrete frames. *J. Struct. Div.* **107**(9), 1713–1729 (1981)
26. Turkish Building Earthquake Code (TBEC), Ministry of public works and settlement. Ankara, Turkey, (2018)
27. Federal Emergency Management Agency (FEMA), Prestandard and commentary for the seismic rehabilitation of buildings. FEMA 356, Washington, DC: Federal Emergency Management Agency, (2000)